# MATHEMATICAL MODELING OF LOOP HEAT PIPES

Tarik Kaya
NRC Resident Research Associate
NASA Goddard Space Flight Center
Jentung Ku
NASA Goddard Space Flight Center
Greenbelt, MD

Triem T. Hoang
TTH Research Inc.
Clifton, VA
Mark K. Cheung
U.S. Naval Research Laboratory
Washington, DC

## ABSTRACT

The primary focus of this study is to model steady-state performance of a Loop Heat Pipe (LHP). The mathematical model is based on the steady-state energy balance equations at each component of the LHP. The heat exchange between each LHP component and the surrounding is taken into account. Both convection and radiation environments are modeled. The loop operating temperature is calculated as a function of the applied power at a given loop condition. Experimental validation of the model is attempted by using two different LHP designs. The mathematical model is tested at different sink temperatures and at different elevations of the loop. The comparison of the calculations and experimental results showed very good agreement (within 3%). This method proved to be a useful tool in studying steady-state LHP performance characteristics.

## NOMENCLATURE

| | |
|---|---|
| $a_R$ | radiator area per length |
| $C_P$ | specific heat at constant pressure |
| $D_{WICK}$ | diameter of wick |
| $k_{EFF}$ | effective thermal conductivity of wick |
| $k_L$ | liquid thermal conductivity of working fluid |
| $k_{WICK}$ | thermal conductivity of wick material |
| $L_C$ | length of condenser tube |
| $L_C^{2\phi}$ | length of two-phase portion of condenser tube |
| $L_{CC}$ | length of compensation chamber |
| $L_{WICK}$ | length of wick |
| $Nu_D$ | Nusselt number |
| $\dot{m}$ | mass flow rate |
| $P_{SAT}$ | saturation pressure |
| $\dot{Q}_{APP}$ | total heat load applied to evaporator |
| $\dot{Q}_C$ | heat rejected by two-phase portion of condenser |
| $\dot{Q}_{CC-A}$ | heat loss/gain between compensation chamber and ambient |
| $\dot{Q}_{HL}$ | heat leak or back conduction |
| $\dot{Q}_{SC}$ | amount of required subcooling |
| $\dot{Q}_{VL-A}$ | heat loss/gain between vapor line and ambient |
| $T_{AMB}$ | ambient temperature |
| $T_R^{2\phi}$ | radiator temperature in two-phase portion of condenser |
| $T_{SAT}$ | saturation temperature of LHP |
| $T_{SINK}$ | sink temperature |
| TL | liquid line temperature |
| $(UA/L)_C^L$ | thermal conductance per unit length in liquid portion of condenser |
| $(UA/L)_{C-A}$ | thermal conductance per unit length from surface of condenser tube to ambient |
| $(UA/L)_{C-S}$ | thermal conductance per unit length from inner surface of condenser tube to outer surface of condenser plate |
| $(UA/L)_{CC-A}$ | thermal conductance per unit length from surface of compensation chamber to ambient |
| x | thermodynamic quality |
| z | axial coordinate |
| $\Delta T_{AC,WICK}$ | temperature difference across wick |
| $\Delta P_{TOTAL}$ | total presssure drop in LHP |
| $\varepsilon$ | wick porosity and emissivity of radiator surface |
| $\lambda$ | latent heat |
| $\eta_R$ | efficiency of radiator surface |
| $\pi$ | 3.141592.... |
| $\sigma$ | Stefan-Boltzman constant |

## INTRODUCTION

Loop Heat Pipes (LHPs) are robust, self-starting and passive two-phase thermal transport devices, which utilize the latent heat of vaporization of a working fluid to transfer heat, and the surface tension forces formed in a fine-pore wick to circulate the working fluid. They are used to transport excess heat from a heat source such as payload instruments in a spacecraft to a low temperature heat sink, while maintaining the temperature within specified limits. As shown in Fig. 1, a typical LHP consists of an evaporator, a reservoir (also called the compensation chamber or hydro-accumulator), vapor and liquid transport lines, a subcooler, and a condenser. The compensation chamber is thermally and hydrodynamically connected to the evaporator. In addition to the primary wick inside the evaporator, in many LHPs, a secondary wick is also used between the compensation chamber and the evaporator to ensure that the primary wick is wetted at all times.

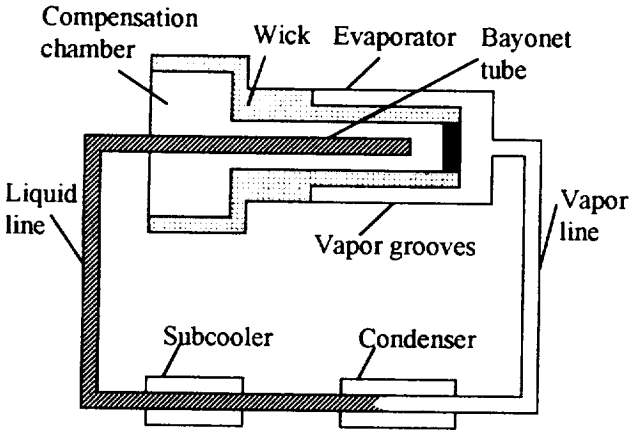


**Fig. 1 Schematic of a LHP (not to scale).**

During a typical LHP operation, the heat is applied to the evaporator. The evaporator absorbs the applied heat. Both the evaporator and the compensation chamber temperatures rise together, indicating a heat leak from the evaporator to the compensation chamber. When the temperature difference between evaporator and the compensation chamber is high enough to provide the required superheat, the boiling starts in the evaporator. The start-up is identified by a sudden drop of the evaporator temperature and a sudden increase of the vapor line temperature. The vapor is collected in the vapor grooves, and pushed into the vapor transport line due to the increased pressure from boiling. The meniscus inside the wick adjusts naturally itself to establish a capillary head that matches the total pressure drop in the loop. The capillary head prevents vapor from penetrating into the wick structure. The vapor is then condensed in the condenser and later subcooled. The subcooler can be an integral part of the condenser. The subcooled liquid returns to the evaporator through the compensation chamber. A detailed thermodynamic analysis of this operation is discussed in Ref. 1.

LHPs can transport large thermal power loads, as much as 1.7 kW, over long distances through flexible and small diameter tubes[2]. A heat flux of 0.70 MW/m$^2$ through the LHP's evaporator has been demonstrated[2]. Start-ups with very low heat loads, as low as 2 W, has been achieved[3]. They can also provide important heat rejection capability even positioned against gravity with an adverse elevation of the evaporator. 1.2 kW against a 4-m adverse elevation was demonstrated. Several ground applications are therefore feasible. The ability of the LHPs to operate against gravity also makes ground testing of space applications possible. It is also possible to implement new technologies such as deployable radiators due to the fact that the flexible sections can easily be incorporated into the LHP's transport lines[4].

The LHP is closely related to the Capillary Pumped Loop (CPL). The CPL requires extensive pre-conditioning of the loop prior to start-up and is susceptible to deprime or loss of pumping action in the evaporator. However, the LHP can be started by directly applying heat to the evaporator, and is largely resistant to the depriming problems caused by the presence of the bubbles in the evaporator core. Although both technologies exhibit extensive design flexibility to accommodate specific thermal control requirements, LHPs are considered to be simpler and more robust devices than CPLs[5].

Altogether, these characteristics make the LHPs very attractive thermal control devices in both ground and space applications. The LHP is currently the baseline design of the thermal control systems for NASA's Goescience Laser Altimeter System (GLAS), some future DoD spacecraft, and next generation large communication satellites. Another application under development is anti-icing system for the aircraft engine cowls using waste engine heat[6]. The ground applications include roof top solar installations and the cooling of remote communication sheds in a hot desert environment by transporting the heat into the ground, the cooling of semiconductor chips and reactors.

LHP was invented in the former Soviet Union in the early 1970s. The first patent was issued by Maidanik in 1985[7]. The first flight test was performed aboard a Russian spacecraft Granat in 1989[8]. During this flight test, the long term and reliable flight operation of LHPs in micro-gravity has successfully been demonstrated. Two successful flight experiments of American Loop Heat Pipe (ALPHA) proved over 56 hours of perfect

on-orbit operation on the STS-83 and STS-94 missions respectively in April and July 1997[9]. Another successful flight test was performed on more recent STS-87 mission in November 1997[9]. Brief surveys of the earlier experimental studies on LHPs are summarized in Refs. 10 and 11.

Because of the complexity of the related two-phase heat transfer phenomena, the LHP modeling efforts have mainly been focused on simplified steady-state energy balance equations. Many of the previous studies have used either oversimplified assumptions, or analyzed only one component of LHP. For some other studies, the main algorithm of the model and the comparison of numerical and experimental results were not revealed. Maidanik et al.[12] developed an analytical model with a closed form solution for the energy and pressure balances. Dickey and Peterson[10] used a simplified steady-state model. Their model shows good agreement with the experimental data obtained at various tilts. However, they limited the input power to less than 170 W. Bienert and Wolf[13] correlated successfully the test data by using an analytical model based on steady-state energy balances. Wirch and Thomas[11] modeled the evaporator section of a LHP by using a two-dimensional finite element method and validated their model experimentally for vapor line temperatures of 40 and 50°C. Several manufacturers have developed LHP models by using SINDA/FLUINT solver[4, 5]. Due to the commercial importance of this recent technology, only a limited amount of test data and information has been published in the open literature.

This study focused on the mathematical modeling of the LHPs. The mathematical model of the LHP was based on the steady-state energy balance equations at each component of the system. The heat exchange between each LHP component and the surrounding –in convection and radiation environments– was taken into account. The results of the model were compared with the experimental results obtained by using two LHPs of different design. The experiments were conducted at different sink temperatures and at different elevations of the LHPs. The comparison between the model predictions and the experimental results showed very good agreement, validating the mathematical model proposed in this study.

## MATHEMATICAL MODEL

The loop operating (saturation) temperature is calculated as a function of the input power at a given loop condition. The specified loop condition includes the sink temperature, the ambient temperature, and the elevation between the evaporator and the condenser. In this section, the calculation algorithm for the convection environment will be presented in detail. The main differences in calculating the radiation environment will briefly be addressed at the end of this section.

The assumptions used in the development of the model are as follows:

1) The mass and heat transfer through the wick is realized only in the radial direction.
2) The compensation chamber and the evaporator core contain both liquid and vapor phases (two-phase fluid).
3) LHP achieves steady state for a given loop condition.
4) Single-phase flow correlations are employed to calculate the pressure drop and the heat transfer film coefficients in the condenser and subcooler.
5) In the convection environment, the heat exchange between the loop components and ambient is assumed to be natural convection.

The liquid-vapor interface can be in the vapor line, the condenser, the subcooler, or the liquid line, depending on the applied heat load and the condenser sink temperature. The model can predict the operating temperature of the loop for both cases: single-phase or two-phase fluid returning to the compensation chamber. If the charging strategy of the loop is such that the compensation chamber is completely filled with liquid when the condenser is totally utilized, the model predictions will not be accurate since only two-phase flow is allowed in the compensation chamber (Assumption 2).

Inputs of the program (loop dimensions such as the lengths of transport lines, the wick properties, the type of working fluid, and the elevation etc.) are stored on a spreadsheet, and they can be easily changed. This allows a fast and simple parametric study of the LHP performance.

The relevant properties of the working fluid are saturation pressure, liquid density, vapor density, liquid viscosity, vapor viscosity, liquid thermal conductivity, liquid specific heat, and surface tension. These fluid properties are functions of the loop operating temperature $T_{SAT}$. Each of these properties is curve fitted into a fifth order polynomial with respect to $T_{SAT}$ with errors of approximately 1-5%. Each fluid property, represented here by a variable Y, is calculated as shown below:

$$Y = \sum_{n=0}^{5} A_n T_{SAT}^n \qquad (1)$$

The coefficients ( $A_n$ ) of the polynomials are given in Ref. 14. The local liquid properties are calculated by using the average temperatures at each element of the loop.

**Solution Procedure**

For a given applied heat load, sink and ambient temperature, and position of the loop, the LHP operating temperature can be calculated by solving the energy balance equations written for each LHP component. To solve these equations, the relevant fluid properties, the system pressure drop, the mass flow rate and the heat transfer coefficients should be known. However, these values are functions of the loop operating temperature. Thus, the system of governing equations is an implicit function of the loop operating temperature, and an iterative solution scheme is required.

In a LHP, the compensation chamber controls the operating temperature of the loop. The compensation chamber temperature is a result of three heat transfer paths: heat exchange between the evaporator and the compensation chamber (also called heat leak or back conduction), heat exchange between the compensation chamber and the environment, and heat exchange between the compensation chamber and the returning liquid (subcooling). Under a steady-state operational condition, the LHP operating temperature adjusts itself such that the condenser generates enough subcooling to match the heat leak and the heat exchange with the environment, which is given by the following equation:

$$\dot{Q}_{HL} = \dot{Q}_{SC} + \dot{Q}_{CC-A} \qquad (2)$$

Heat Leak across the Wick. The heat leak $\dot{Q}_{HL}$ from the high pressure side of the wick to the low pressure side is transferred through conduction, which can be written as:

$$\dot{Q}_{HL} = \frac{2\pi k_{EFF} L_{WICK}}{\ln(D^{OUT}_{WICK} / D^{IN}_{WICK})} \Delta T_{AC,WICK} \qquad (3)$$

The heat exchange between the returning subcooled liquid and the wick material causes a nonlinear profile. However, this is a small effect and can be neglected. The temperature difference across the wick $\Delta T_{AC,WICK}$ is the difference between the local saturation temperatures caused by the total system pressure drop, excluding the pressure drop in the wick structure:

$$\Delta T_{AC,WICK} = \left(\frac{\partial T}{\partial P}\right)_{SAT} (\Delta P_{TOTAL} - \Delta P_{WICK}) \qquad (4)$$

The slope of the vapor-pressure curve $(\partial T/\partial P)_{SAT}$ can be calculated using the Clausius-Clapeyron relation. However, since the fluid properties are curve fitted into fifth-order polynomials with respect to $T_{SAT}$, the slope $(\partial T/\partial P)_{SAT}$ can be more accurately predicted if it is differentiated from the functional relationship between $P_{SAT}$ and $T_{SAT}$, which is given in the form of Eq. (1)[14].

Total System Pressure Drop of the LHP. The total system pressure drop $\Delta P_{TOTAL}$ in Eq. (4) is a function of the loop operating temperature, the location of liquid-vapor interface in the condenser (which depends on the sink and ambient temperatures), and the amount of heat transported to the condenser.

The total system pressure drop consists of the frictional steady-state pressure drops in the vapor and liquid lines, the condenser, the subcooler, and the evaporator. The pressure drop in the evaporator includes those in the bayonet tube, the wick structure, and the vapor grooves. If the loop is positioned with an elevation against gravity, the pressure difference due to the gravitational forces should also be taken into account. Thus, the total system pressure drop is the sum of the pressure drops at each LHP element:

$$\Delta P_{TOTAL} = \Delta P_{VL} + \Delta P_{LL} + \Delta P_{C} + \Delta P_{SC} + \Delta P_{BAY} + \Delta P_{WICK} + \Delta P_{V.GR.} + \Delta P_{GRAV.} \qquad (5)$$

The calculation of the pressure drop constitutes an important part of the model since the temperature drop, thus the heat leak from the evaporator to the compensation chamber, is directly related to the pressure drop. Single-phase correlations are employed to calculate the pressure drop. The laminar and turbulent flow regimes are taken into account in these correlations. When calculating the pressure drop in the evaporator, the effective length of the vapor grooves and the liquid core is taken as the half of the evaporator active length.

Effective Thermal Conductivity of the Wick. Two different correlations are used to calculate the effective thermal conductivity of the wick to analyze the influence of the different correlations on results. For the first correlation, the effective thermal conductivity of the wick is obtained by volume averaging the thermal

conductivity of the wick material and the working liquid:

$$k_{EFF} = k_{WICK}(1-\varepsilon)+\varepsilon k_L \qquad (6a)$$

This correlation is substituted by the following correlation, proposed by Dunn and Reay[15]:

$$k_{EFF} = k_{WICK}\left(\frac{2+(k_L/k_{WICK})-2\varepsilon(1-(k_L/k_{WICK}))}{2+(k_L/k_{WICK})+\varepsilon(1-(k_L/k_{WICK}))}\right) \qquad (6b)$$

Heat Transfer Coefficients. The thermal conductances of the condenser and the subcooler are calculated by considering the thermal resistance network shown in Fig. 2.

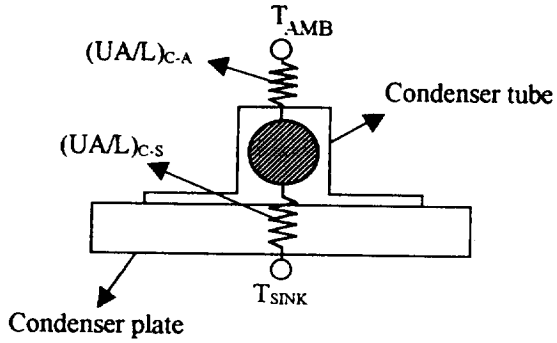


**Fig. 2 Schematic of the condenser thermal resistance network.**

In the convection environment, the heat exchange between the loop and the ambient is assumed to be natural convection. The simplified natural convection correlations for air from Ref. 16 are used to calculate the heat transfer coefficients from the loop element surfaces to ambient. The thermal conductance from the inner surface of the condenser tube to the external surface of the condenser plate is computed by considering the flow arrangement of the heat exchanger. The convective film coefficient due to the fluid flow inside the condenser tube is calculated as a function of the operating temperature.

As an example, the heat film coefficient per unit length in the liquid portion of the condenser tube is calculated by using the following thermal network:

$$(UA/L)_C^L = 1/[1/(UA/L)_{C-S} + 1/(\pi Nu_D k_L)] \qquad (7)$$

The first term in the left side of the Eq. (7) is computed by considering the thermal resistances for conduction for a given condenser geometry. The thermal contact resistance between the loop and the condenser plate should also be taken into account. For the second term, the Nusselt number $Nu_D$ is constant for a laminar and fully developed flow and equal to $Nu_D = 4.36$ if the surface heat flux is constant, and $Nu_D = 3.66$ if the surface temperature is constant[17]. The liquid thermal conductivity $k_L$, is known as a function of the loop operating temperature.

Return Liquid Subcooling. The heat rejected in the two-phase portion of the condenser $\dot{Q}_C$ can be written as:

$$\dot{Q}_C = \dot{Q}_{APP.} - \dot{Q}_{HL} - \dot{Q}_{VL-A} \qquad (8)$$

The heat exchange between the vapor transport line and ambient can be positive or negative depending on the sink and ambient temperatures. The two-phase heat removal in the condenser tube consists of two parts: heat rejection to the sink and heat loss to ambient. Thus, the length of the two-phase flow portion in the consider is given by:

$$L_C^{2\phi} = \dot{Q}_C \int_{x_{IN}}^{x_{OUT}} \left\{ \frac{dx}{\left[ (UA/L)_{C-S}(T_{SAT}-T_{SINK}) + \right.} \right.$$

$$\left. \left. \frac{}{(UA/L)_{C-A}(T_{SAT}-T_{AMB})} \right] \right\} \qquad (9)$$

The related convective film coefficients in the parenthesis are calculated by considering the thermal resistance network of the each heat transfer path, as explained in the section above. If the result of the integration of Eq. (9) with respect to the quality from $x_{IN}=1$ to $x_{OUT}=0$ is less than the total length of the condenser, the liquid-vapor interface is situated inside the condenser. Otherwise, the same calculation methodology is used to compute the location of the liquid-vapor first in the subcooler, and then in the liquid line.

Since the length of the two phase flow portion in the condenser is calculated, it is now possible to calculate the liquid temperature at the condenser exit by integrating the energy balance equation in the liquid

portion of the condenser, i.e.:

$$\frac{Q_C}{\lambda} C_p \frac{dT}{dz} = (UA/L)_{C-A}(T - T_{AMB}) + (UA/L)_C^L (T - T_{SINK}) \quad (10)$$

If the loop contains an additional subcooler unit, the Eq. (10) can be applied to the subcooler to calculate the exit temperature. Similarly, the same equation is valid to calculate the liquid line exit temperature. Thus, the amount of return liquid subcooling is given by:

$$\dot{Q}_{SC} = \dot{m} C_p (T_{SAT} - TL_{OUT}) \quad (11)$$

LHP Operating Temperature. The heat loss or gain between the compensation chamber and ambient through natural convection can be written as:

$$\dot{Q}_{CC-A} = (UA/L)_{CC-A} L_{CC} (T_{SAT} - T_{AMB}) \quad (12)$$

By substituting Eqs. (3), (11) and (12) into Eq. (2), one will obtain the following equation:

$$F_1(T_{SAT}, T_{SINK}, T_{AMB}, \dot{Q}_{APP.}) = F_2(T_{SAT}, T_{SINK}, T_{AMB}, \dot{Q}_{APP.}) + F_3(T_{SAT}, T_{AMB}) \quad (13)$$

where $F_1, F_2,$ and $F_3$ are known functions. For given $T_{SINK}, T_{AMB},$ and $\dot{Q}_{APP.}$, the LHP operating temperature can be determined by solving Eq. (13) iteratively for $T_{SAT}$. The convergence is assumed to occur when $|F_1 - (F_2 + F_3)| < 10^{-3}$ W. To accelerate the convergence of the solutions, the estimation of the operating temperature at each iteration is corrected as a function of the residual of Eq. (13). A typical converged solution for a given heat load is reached at approximately 1000 iterations. It takes approximately 5 seconds to reach a converged solution at a given power level by using a 120 MHz Pentium processor.

**Radiation Environment**

The general algorithm used to calculate the radiation environment is the same as that of the convection environment. When the liquid-vapor interface is in the condenser, the heat removal by radiation in the two-phase portion of the condenser can be written as follows:

$$\dot{Q}_C = (UA/L)_{C-S}(T_{SAT} - T_R^{2\phi}) L_C^{2\phi} - \sigma \varepsilon_R a_R \left[ \left( T_R^{2\phi} \right)^4 - \left( T_{SINK} \right)^4 \right] L_C^{2\phi} \quad (14)$$

The radiator temperature $T_R^{2\phi}$, and the length of the two-phase portion of the condenser $L_C^{2\phi}$ can be calculated by using Eq. (14). Similarly, the other heat exchange relations between the loop components and environment should be replaced by the radiation heat transfer equations. The calculation of the return liquid subcooling follows the same method as that of the convection environment.

## EXPERIMENTAL SETUP AND PROCEDURE

Two separate test programs were conducted at NASA Goddard Space Flight Center (GSFC) to verify the mathematical model. In the first test program, a LHP designed for the thermal control of the Goescience Laser Altimeter System (GLAS) spacecraft was used. The second test program was performed on a research LHP designed for the Naval Research Laboratory (NRL). A complete discussion on the performance characteristics of each LHP can be found in Refs. 18 and 19. Only a brief description of each LHP will be given in this section.

**Instrumentation and Test Procedure**

To monitor the temperature profiles of the loop and environment, more than 45 copper/constantan (type T) thermocouples were placed at critical locations of the each LHP. The uncertainty of the thermocouple readings was estimated to be ± 0.5 K.

The heat source consisted of cartridge and tape heaters. The cartridge heaters were used for high power tests and they can provide up to 1 kW of electrical power. Two types of tape heaters were employed with maximum electrical powers of 200 W and 700 W. Heaters were mounted either on only one side or on each side of the evaporator section. Tape heaters were attached to the compensation chamber to control the set point temperature for some of the tests. Relays and variacs were used to control the heaters. The uncertainty in measuring the power input was estimated less than 2%.

The condenser lines were coupled to a cold [ethlyene glycol (60%) / water (40%)] heat rejection system with a 1.5 kW cooling capacity. All measurements were taken with a computerized data acquisition system. Data were displayed in real time and stored to be analyzed later. Sampling rate was 10 kHz with a

resolution of 16-bit and an ADC system accuracy of 0.6%.

During a typical test, the first step was to set the chiller temperature at a desired value. Once the condenser reached a steady state, the power was applied to the evaporator. At each power level, the system was allowed to reach steady state. This would take more than 5 hours at low powers (<100W) and approximately half an hour at high powers. Tests were performed by cycling the power and the sink temperature at various positive and adverse tilts, and elevations.

## Characteristics of LHP1 (GLAS LHP)

GLAS spacecraft was designed to obtain ice sheet and ocean topography, and global profiles of land and vegetative canopy. GLAS utilizes three lasers, each of which dissipates approximately 100 W when operating, and only one laser is needed at a time. A heat pipe/LHP system was proposed for thermal control. A prototype LHP was manufactured by Dynatherm Corporation, Inc. GLAS LHP (LHP1) has a cylindrical evaporator with a diameter of 25.4 mm and a length of 150 mm. The evaporator's envelope is constructed of low carbon steel, and it uses a sintered nickel wick with an effective pore radius of less than 1.2 micron. A copper saddle is attached to the evaporator's envelope to hold three cartridge heaters. The compensation chamber has a diameter of 46 mm and a length of 76 mm. Both the liquid and vapor transport lines are approximately 460 mm long each. They are made from smooth wall tubing with a diameter of 5.54 mm and a wall thickness of 0.51 mm. The condenser is a single pass, direct condensation heat exchanger type with a total length of 4.06 m and a diameter of 5.54 mm. It is made from an extruded small diameter aluminum tubing with an integral fin. The condenser tubing is bent into serpentine shape, which makes passes across a radiator panel. The heat exchanger is mounted to the radiator panel similar to that proposed for GLAS.

## Characteristics of LHP2 (NRL LHP)

The NRL LHP (LHP2) has a cylindrical evaporator of 25.4 mm in diameter and 305 mm in length. The compensation chamber has the same diameter as the evaporator, and is 60 mm long. A sintered nickel wick with an effective pore radius of less than 1.2 micron is used. The liquid and vapor transport lines are made of 4.8 mm outer diameter stainless steel tubing, and has an overall length of about 1524 mm each. The condenser consists of three separate sections linked in series. It is made up of 4.8 mm outer diameter stainless steel tubing with an overall length of 2032 mm. The condenser is similar to that of LHP1 (i.e. single pass and direct condensation heat exchanger). However, no radiator panel is employed. The condenser line is attached to the coolant loop by small aluminum saddles and epoxy fillings are used between the tubes to minimize the thermal contact resistance. The evaporator is embedded into an aluminum saddle so that heat could spread evenly on the upper side of evaporator.

## DISCUSSION OF RESULTS

Results are presented on the LHP performance curve (applied power versus operating temperature). Figure 3 shows the comparison between the experimental results and the predictions for LHP1.

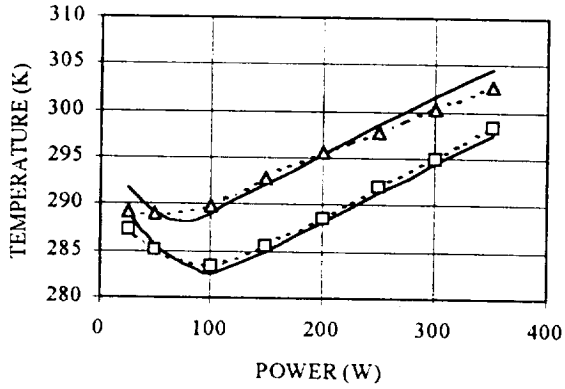


**Fig. 3 Comparison of experimental results and model predictions for LHP1. Δ, measurements for $T_{sink}$=273 K; □, measurements for $T_{sink}$=283 K; ——— predictions.**

The experimental results were obtained at eight different power levels for two distinct sink temperatures of 273 K and 283 K. The condenser plate was in vertical position such that the evaporator and the compensation chamber were leveled horizontally within ± 2.5 mm. The calculations are between 0.1 and 1% of the experimental measurements. As shown in Fig. 3, at lower powers (approximately less than 100 W), the operating temperature decreases with increasing power due to the cold liquid returning from the condenser. In this region, the LHP is in the variable conductance mode. At a certain power, the condenser becomes completely open and the LHP operates in the constant conductance mode. At this point, the operating temperature starts increasing almost linearly with the applied power. The operating temperature predictions at low powers are less satisfactory (between 0.3 and 1%). This is due to the fact that the effect of the heat exchange with ambient is more pronounced at low powers. More precise correlations than simplified natural convection equations are required to improve

the results in this region. The operating temperature predictions at low powers were also less accurate in Ref. 13, due to probably the same difficulty in modeling the heat exchange between the compensation chamber and ambient. At higher powers, the energy balance is dominated by the liquid returning from the condenser rather than the heat exchange with ambient. The heat exchange with ambient becomes a smaller fraction of the applied heat (e.g. 1.2% at 25 W and 0.2% at 200 W). As a result, the predictions are better at high powers (within 0.2%).

As shown in Fig. 3, when the sink temperature is increased from 273 K to 283 K, the loop performance curve shifts towards higher operating temperatures. The lowest operating temperature on the curve also shifts towards lower power levels since less subcooling is provided when the sink temperature gets closer to the ambient temperature. When the sink temperature is equal to ambient temperature, there is no additional subcooling available and the loop operates entirely in the fixed conductance mode. This condition can be simulated by this mathematical model.

The corresponding total pressure drop in the loop and the mass flow rate as a function of the applied power is shown in Fig. 4 for the sink temperature of 283 K.

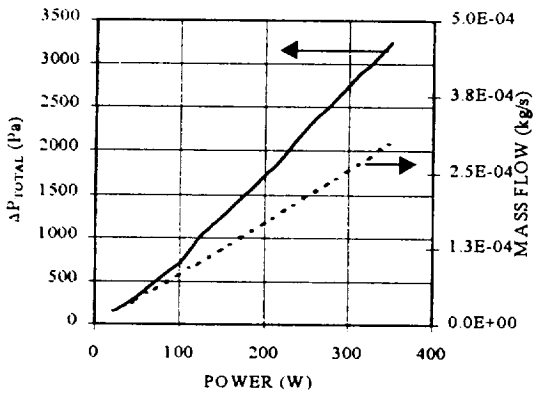


**Fig. 4 Calculated total pressure drop and mass flow rate curves for LHP1 at $T_{sink}$=283 K.**

Both values increase as a function of the applied power. The sudden increase of the total pressure drop around 100 W is due to the transition from the laminar to the turbulent flow regime. It can also be seen that the mass flow rate is very small at low powers. Therefore, little cooling is provided to the compensation chamber. This is consistent with the earlier statement that the influence of the subcooled returning liquid becomes important as the power increases.

Two different correlations for the wick thermal conductivity (Eqs. 6a and 6b) were used to study the influence of the correlations on the results. The difference in the operating temperatures was less than 0.03%, suggesting that either of these two correlations can be used within the operation limits of interest.

Figure 5 shows the result obtained by using LHP2. The experimental results were obtained by using seven different power profiles (from A to E). The power profiles for each cycle are given in Table 1. Each power cycle from A to E took approximately 10 hours to be completed, and the power cycle E took approximately 72 hours. This was due to the long waiting times at each power to reach the steady-state operation.

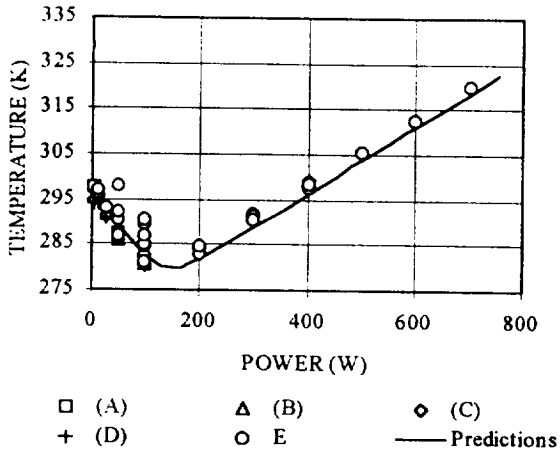


**Fig. 5 Comparison of experimental results and model predictions for LHP2 at $T_{sink}$=263 K.**

The ambient temperature change during these tests was approximately 2 degrees, and an average ambient temperature was used in the calculations for all the cycles. All the tests were conducted with a sink temperature of 263 K and the LHP was leveled horizontally within ± 2.5 mm such that the evaporator, the compensation chamber and the condenser were in the same horizontal plane.

**Table 1 Power profiles for different test cycles.**

| Cycle | Power profile (W) |
|---|---|
| A | 50-5-50 |
| B | 2-10-25-50-10 |
| C | 5-10-25-50-100-50-25 |
| D | 5-10-25-50-100-200-300-400-300-200-100-200 |
| E | 10-25-50-100-200-300-400-300-200-100-50-400-50-100-200-300-400-100-700-100-50-100-200-100-700-600-500-400-300-200-100-50 |

During these power cycling test, a temperature hysteresis was observed at power levels less than 200 W. This phenomenon was discussed in detail in Ref. 19. When the power was decreased with a moderate step

change (less than 100 W) the operating temperatures values were stable. However, when the power was decreased with a higher step, the loop operating temperatures were deviated from their initial steady-state values at a given power. The scattered points at low powers presented in Fig. 5 are due to this temperature hysteresis phenomenon. The model predictions were between 0.7-2.7% of the experimental measurements when the power steps were small enough such that no temperature hysteresis was observed. It is obvious that the analytical model used in this study cannot predict the temperature hysteresis. At high powers, the temperatures were very stable regardless of the power cycling profile, and the model predictions were very satisfactory.

The analytical model was also tested when the loop was positioned at an elevation with the evaporator and the compensation chamber leveled horizontally above the condenser. A typical comparison is presented in Fig. 6 for an elevation of 660 mm (vertical distance between the evaporator axis and the lowest point of the loop). The experimental results were obtained by using the power cycle E given in Table 1.

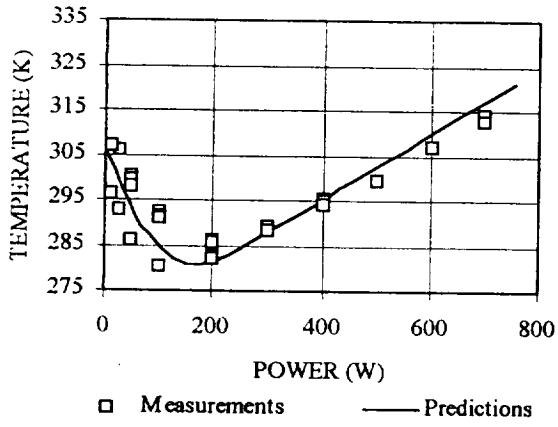


**Fig. 6 Comparison of experimental results and model predictions for LHP2 at $T_{sink}$=263 K and an elevation of 660 mm.**

The comparison of the experimental results and the calculations were again more satisfactory at high powers (within 1.5%). The temperature hysteresis is clear at low powers. At high elevations, it was found that the operating temperatures were shifted to an upper curve when the power was cycled up and down, and stayed stable on this upper curve. The analytical model predicted well the overall tendency of the LHP performance curve at low powers as shown in Fig. 6.

## SUMMARY AND CONCLUSIONS

An analytical model for the steady-state LHP operation was presented. The analytical model was tested with two separate LHP designs at different sink temperatures and different elevations. The calculations were within 3% of the experimental measurements, indicating that the steady-state LHP performance was correctly modeled. The predictions were less satisfactory at low power regions (less than approximately 100 W), where the heat exchange with ambient influences more the energy balance of the compensation chamber. Agreement could be improved by using more precise correlations for calculating the natural convection heat transfer coefficients. Another important observation at low powers was the temperature hysteresis of LHP2. The model cannot predict the temperature hysteresis, however; the calculations appear to be in good accord with the experimental results. As a result, the model can be used for a reasonable assessment of the LHP performance even in the presence of the temperature hysteresis.

The temperature hysteresis phenomenon has not been well understood, and it is currently under investigation. A better understanding of the physical mechanism behind the temperature hysteresis is required for its modeling. Since the start-up and related transients constitute a very important problem of the two-phase devices, the consideration of the unsteady effects is also needed to improve the usefulness of the analytical model.

## ACKNOWLEDGMENTS

This work was performed at NASA Goddard Space Flight Center (GSFC) and the test article LHP2 was on loan from the Naval Research Laboratory (NRL). A part of funding for this work was provided by National Research Council (NRC)-NASA/GSFC Research Associateship Grant.

## REFERENCES

[1] Ku, J., "Thermodynamic Aspects of Capillary Pumped Loop Operation," AIAA Paper 94-2059, June 1994.

[2] North, M., Sarraf, D., Rosenfeld, J., Maidanik, Y., and Vershinin, S., "High Heat Flux Loop Heat Pipes," Conference #970115, American Institute of Physics, New York, 1997, pp. 561-566.

[3] Kaya, T., Ku, J., Hoang, T. T., and Cheung, M. K., "Investigation of Low Power Start-Up Characteristics of A Loop Heat Pipe," STAIF-99, American Institute of Physics, New York, January 1999.

[4] Lashley, C., Krein, S., and Barcomb, P., "Deployable Radiators –A Multi-Discipline Approach," SAE Technical Paper Series, Paper #981691, July 1998.

[7] Nikitkin, M., and Cullimore, B., "CPL and LHP Technologies: What are the Differences, What are the Similarities?," SAE Technical Paper Series, Paper #981587, July 1998.

[8] Phillips, A. L., and Gernert, N. J., "Loop Heat Pipe Anti-Icing System for UAV," IECEC-98-240, August 1998.

[9] Maidanik, Y. F., Vershinin, S., Kholodov, V., and Dolggirev, J., "Heat Transfer Apparatus," U.S. Patent 4515209, May 1985.

[10] Maidanik, Y. F., Fershtater, Y. G., Goncharov, K. A., "Capillary Pumped Loop for the Systems of Thermal Regulation of Spacecraft," *Proceedings of the 4th European Symposium on Space Environmental and Control Systems*, ESA SP-324, December 1991.

[11] Bienert, W. B., "Loop Heat Pipe Flight Experiment," CP420, American Institute of Physics, New York, 1998, pp. 511-513.

[12] Dickey, J. T., and Peterson, G. P., "An Experimental and Analytical Investigation of the Operational Characteristics of a Capillary Pumped Loop," *Journal of Thermophysics and Heat Transfer*, Vol. 8, No. 3, 1994, pp.602-607.

[13] Wirsch, P. J., and Thomas, S. K., "Performance Characteristics of a Stainless Steel/Ammonia Loop Heat Pipe," *Journal of Thermophysics and Heat Transfer*, Vol. 10, No. 3, 1996, pp.326-333.

[14] Maidanik, Y. F., Fershtater, Y. F. and Solodovnik, N. N., "Design and Investigation of Regulation of Loop Heat Pipes for Terrestrial and Space Applications," SAE Technical Paper Series, Paper#941407, June 1994.

[15] Bienert, W. B., and Wolf, D. A., "Temperature Control with Loop Heat Pipes: Analytical Model and Test Results," *Proceedings of the 9th International Heat Pipe Conference*, Los Alamos National Laboratory, May 1995.

[16] Brennan, P. J., and Kroliczek, E. J., "Heat Pipe Design Handbook," NASA Contract NAS5-32406, Vol.2, MD, June 1979, pp. 62-67.

[17] Dunn, P. D., and Reay, D. A., *Heat Pipes*, 3rd ed., Pergamon Press, Oxford, 1982.

[18] Holman, J. P., *Heat Transfer*, 4th ed., McGraw Hill, 1977, p. 253.

[19] Incropera, F. P., and De Witt D. P., *Fundamentals of Heat and Mass Transfer*, 3rd ed., Wiley, New York, 1990, p. 491.

[20] Douglas, D., Ku, J., and Kaya, T., "Testing of the Geoscience Laser Altimeter System (GLAS) Prototype Loop Heat Pipe," AIAA Paper 99-0473, January 1999.

[21] Cheung, M. K., Hoang, T. T., Ku, J., and Kaya, T., "Thermal Performance and Operational Characteristics of Loop Heat Pipe (NRL LHP)," SAE Technical Paper Series, Paper #981813, July 1998.